Chapter 9

Applications

Lattices appear naturally in rather different domains of natural science and formal mathematics. The goal of the present chapter is to discuss briefly several examples of problems which are tightly related with the lattice constructions, lattice classifications, and use lattices as an initial point for more elaborated mathematical and physical models and processes.

9.1 Sphere packing, covering, and tiling

One of the most simply formulated practical problem leading to the study of lattices is the classical problem of packing spheres (or balls). We can think about canon balls or about oranges of the same dimension and try to find the packing that maximizes the density assuming that the dimension of the box to pack the balls is infinitely bigger than the ball dimension. To make this "practical" problem more mathematically sound we can generalize it to an arbitrary dimension and to look for solutions for more restricted problem by imposing the periodicity condition on packing (lattice packing) and more general packing without periodicity.

The solution of this problem is trivial in dimension 1 (see Figure 9.1). One-dimensional spheres ($\sim$ intervals) fill completely one-dimensional space (line).

The solution for the dimension two is also simple (we need to pack disks on the plane, see Figure 9.2). Each disk can be surrounded by six neighboring discs. Continuing this local packing we get the hexagonal lattice which is the densest packing of the 2-D discs.

The density of hexagonal packing can be easily calculated by noting that for discs of radius R, each elementary cell is a rhomb with diagonals equal 2R and $2\sqrt{3}R$. The area occupied by the disk in each elementary cell is equal exactly to the area of one disk, πR^2 (two sectors of $2\pi/6$ and two sectors of $2\pi/3$). The area of the elementary cell is $2\sqrt{3}R^2$. Thus the density is $\pi/(2\sqrt{3}) \approx 0.9069$.

FIG. 9.1 – Densest packing of 1-dimensional spheres on a line.

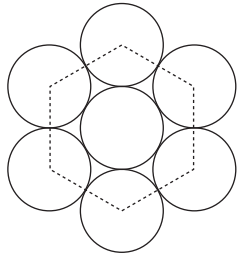

FIG. 9.2 – The most dense packing of two-dimensional spheres (discs) on a plane is a hexagonal lattice packing.

In dimension three the problem of sphere packing is less trivial. The origin of the difficulty can be easily understood if we take one ball and try to put around it the maximal number of identical balls touching it. It is easy to check that it is possible to put 12 balls in contact with one ball but there is still some free space between 12 balls and they can move rather freely being always in contact with the central ball. It is not easy to prove that it is impossible to put the thirteenth ball in contact with the central one. The contact number (i.e. the maximal number of balls which can be put in contact with one ball) is not known for the majority of dimensions $d \geq 4$. It is known that contact numbers in dimensions 8 and 24 are respectively 240 and 196560. These solutions are known because in dimensions 8 and 24 the arrangement of balls around one central ball is unique. These arrangements correspond to the lattice E_8 and to one of the forms of the 24-dimensional Leech lattice.

At the same time it is easy to suggest the packing for 3-D balls (in fact even infinity different versions) which can be thought to be the densest packing. We can start with one layer of balls forming a hexagonal 2D-lattice. Then the next layer can be posed in such a way as to put balls in cavities of the second layer, and so on .... As soon as the number of cavities is twice the number of balls there are two ways to position the next layer. The periodic structure with the shortest period corresponds to the sequence of layers $ABAB\ldots$ This packing is named the hexagonal close packing. The periodic packing of the form $ABCABC\ldots$ corresponds to the structure named face-centered cubic lattice (see Figure 9.3). The density of all packings corresponding to any sequence (periodic or not) of hexagonal layers is $\pi/\sqrt{18}$. Each ball in these packings has 12 neighbors. Although there exist a number of different proofs that the mentioned above packings are the densest ones among lattice packings, only

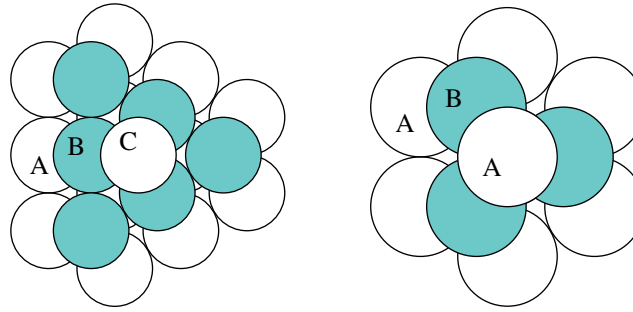

FIG. 9.3 – *ABC* and *ABA* packing of hexagonal layers of balls.

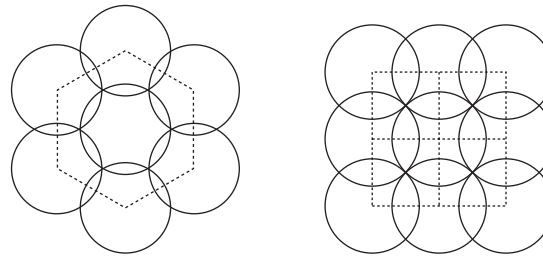

FIG. 9.4 – Covering plane by discs. Center of discs form hexagonal (left) and square (right) lattice. Hexagonal covering is less dense than the square lattice covering.

recently has a computer assisted proof appeared that this statement remains valid for arbitrary non-lattice packings in three-dimensional space.

Nowadays, the solution for the densest packing of spheres is known in many dimensions. The density of the known densest packing varies with dimension in rather irregular fashion. It is also not clear in advance what kind of lattice corresponds to the densest packing for a given dimension.

A problem tightly related to packing is the covering by spheres. Now it is necessary to find the arrangement of overlapping spheres covering the whole space and having the lowest density. The answer is again trivial for the one-dimensional problem. For the two-dimensional problem the hexagonal lattice gives again the best solution (the lowest density) for the covering problem. Figure 9.4 shows the comparison of the coverings obtained for the square lattice and for the hexagonal lattice. For the hexagonal lattice the overlapping of spheres is smaller and the density of covering is lower, namely $2\pi/(3\sqrt{3}) \approx 1.2092$ whereas for the square lattice the density of covering is $\pi/2 \approx 1.5708$.

For three-dimensional lattices the lowest density covering is given by a body-centered lattice, in spite of the fact that the densest sphere packing is associated with another, face-centered cubic lattice.

TAB. 9.1 – Classes of the symmetry groups H of mesomorphic phases of matter: $[E(3) : H]$ compact, H_0 = largest connected subgroup of H, $T_H = H \cap T$, where T is the translation subgroup of $E(3)$.

Class	T_H	H_0
Ordinary nematics	R^3	$R^3 \times U(1)$
Exceptional nematics	R^3	R^3
Cholesterics (chiral)	$R^2 \times Z$	R^3
Smectics A	$R^2 \times Z$	$R^2 \times U(1)$
Smectics C	$R^2 \times Z$	R^2
Chiral smectics C	R^2	R^2
Rod lattices (e.g., lyotropics)	$R \times Z^2$	R
Crystals	Z^3	$\{1\}$

The problem of ball packing can be formulated in a much wider sense than simply as a problem of the densest sphere packing. From the point of view of the description of packing of atoms or molecules in crystals it is natural to ask about regular or lattice packing of balls which are stable in a certain sense (see [11, 5]).

9.2 Regular phases of matter

We want to discuss here briefly the relation of lattices to the classification of different phases of matter, which is more general than just the classification of crystals. In fact, a simultaneous discussion of different mesomorphic phases of matter was suggested by G. Friedel in 1922 [55]. He suggested to treat both crystals and liquid crystals on the basis of symmetry arguments. We follow here the description of the mesomorphic phases of matter done by Louis Michel in [71] on the basis of the symmetry breaking scheme applied to $E(3)$, the three-dimensional Euclidean group. The idea of this classification is to describe the possible stabilizers (little groups in physical terminology) of transitive states. The equilibrium states of matter are associated with the symmetry group which is a subgroup H of $E(3)$. The classes of the symmetry groups H of mesomorphic states of matter are listed in Table 9.1.

Symmetry groups H are defined up to conjugation. When H is discrete, the phase is a crystal. The characteristic lengths of the crystal is not of importance for physical applications, but the difference between left-handed and right-handed crystals can be eventually important for certain physical properties. This is the reason to classify crystals up to a conjugation in the connected affine group (see section 8.3). This yields 230 crystal symmetries. The same classification principle leads to an infinity of other H subgroups. They can be

put in families according to the topology of their largest connected subgroup H_0 and their intersection $H \cap T = T_H$ with the translation subgroup of $E(3)$. These broad classes are listed in Table 9.1.

Short description of the most important other mesomorphic phases is as follows.

In nematics, the molecules are aspherical; their positions are distributed at random as in a liquid, but they are aligned. In ordinary nematics H is the semidirect product $R^3 \wedge D_{\infty h}$. This means that the orientation of the molecules causes them to yield only axially symmetric quadrupole effects even when the molecules have no axial symmetry. Near the solidification temperature, molecules with strong deviation from axial symmetry may rotate less easily and exceptional nematics can be observed (e.g. birefringent quadrupoles with three unequal axes).

Cholesterics are constructed of polar molecules; their symmetry group H contains all the translations in a plane and, with a perpendicular axis, a continuous helicoidal group. They appear frequently in biological tissues.

In smectics the molecules are distributed in parallel monomolecular or bimolecular layers, and they are aligned either perpendicularly (smectics A) or obliquely (smectics C) to the layers. In chiral smectics C inside each layer the polar molecules are oriented with a constant oblique angle, but the azimuth of this orientation turns by a constant angle θ from one layer to the next and two different subclasses are possible depending on whether θ/π is rational or not.

The classification of mesomorphic phases of matter described above is based on the spatial distribution of atomic positions with each atom being represented as a point in real physical space. Naturally, the points representing the localized atoms in space are associated with heavy atomic nuclei (eventually together with some internal electrons), whereas (outer) electrons are distributed in space in the presence of the lattice formed by localized atomic cores.

From the physical point of view it is quite interesting and important to find if there are some more general restrictions which allows us to introduce some universality classes of matter which persist even if periodicity is broken. It is possible to look for such criteria which are due to global topological effects (invariants) which cannot be removed under small deformation breaking symmetry. Classification of universal classes of topological states of matter takes into account the global symmetries like time reversal, charge conjugation, and their combination. The origin of particles themselves (fermions or bosons) is equally important. This subject has become very popular now due to the discovery of such new topological phases of matter as topological insulators or topological superconductors [27].

9.3 Quasicrystals

We cannot avoid to mention the application of lattice geometry to study quasicrystals, or aperiodic regular structures. This is mainly due to the fact that aperiodic crystals can be naturally described as projections of a higher dimensional periodic structure to a subspace of lower dimension. In order to obtain an aperiodic structure the subspace on which such a projection is realized should be irrational with respect to the lattice vectors of the initial periodic structure. Such a construction justifies the interest in the study of higher dimensional periodic structures but creates at the same time a lot of questions about the relevance of the choice of the dimension and of the orientation of the subspace to project the structure. We do not enter in this very popular domain which has a lot of applications not only in the analysis of quasicrystals (fully recognized as an important class of physical systems by awarding the Nobel prize for their discovery in 2011) but in various different branches of physics and mathematics, including chaotic dynamical systems, singularity theory, etc. For an introduction to quasicrystals and related mathematical domains see [17, 24].

9.4 Lattice defects

The classification of the mesomorphic states of matter uses an idealization that the ordered phase of matter is extended indefinitely in space in order to be globally invariant under an allowed subgroup H of $E(3)$. This idealization is not bad if the real sample under study is large enough (as compared to the size of the unit cell) so that its symmetry can be recognized. But, in nature, samples are not only limited in size, but they also can be non-perfect, i.e. they can have defects.

Application to physically real objects of lattice theory is related to the description and classification of typical defects and boundaries. The first step in defect description should include the description of so called topologically stable defects, which persist in the medium even under small (local) deformation.

A very intuitive and visual description of possible defects in regular (periodic) physical materials (crystals, liquid crystals) is based on the "cut and glue" construction of defects for regular lattices.

We give below several examples of such defect constructions. The simplest defect is a vacancy which corresponds to removing one vertex of the lattice without qualitatively disturbing the surrounding (see Figure 9.5, left). This means that testing the lattice locally in any region outside of a small neighborhood of a vacancy we cannot notice the presence of the defect.

A more complicated defect, linear dislocation, is shown in Figure 9.5, center and right. To construct such a defect we remove (we can also insert) one ray of points (eventually several parallel rays) and glue the two boundaries of

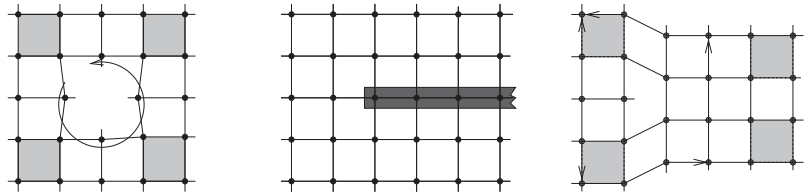

FIG. 9.5 – Lattice with a vacation (left). Construction of a linear dislocation (center). Lattice with a linear dislocation (right).

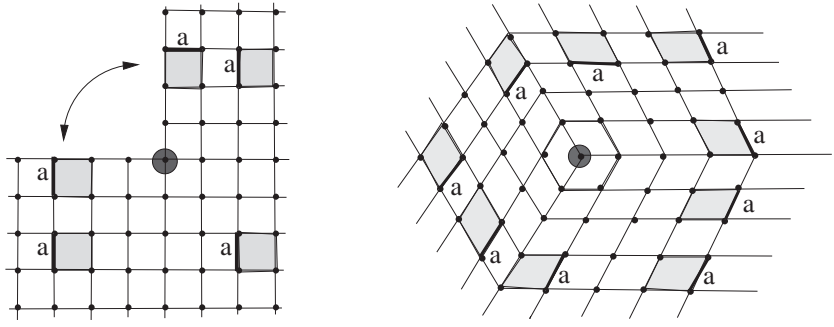

FIG. 9.6 – Construction of the rotational disclination by removing the solid angle $\pi/2$ shown on the left picture.

the cut by a parallel translation along the transversal direction. For the two-dimensional lattice the linear dislocation results in a point (codimention-2) defect. But the evolution of the elementary cell along a closed path surrounding the defect does not modify the elementary cell. In order to characterize the linear dislocation we can introduce the Burgers vector which characterizes what happens with the closed contour chosen on the initially perfect lattice after constructing the dislocation.

The next important defect of the regular lattice is the rotational disclination. We can get it by removing (or adding) an angular wedge from the regular lattice and then joining the two boundaries by rotating them. Examples of such a construction of $\pi/2$ and π rotational disclinations are shown in Figures 9.6 and 9.7. The effect of the evolution of the elementary cell along a closed path surrounding the rotational disclination consists in rotation of the elementary cell by an angle associated with rotational disclination.

We need to distinguish rotational disclination from the angular dislocation shown in Figure 9.8. Angular dislocation is less typical as a defect of real crystals but it turns out to be of primary importance in integrable dynamical

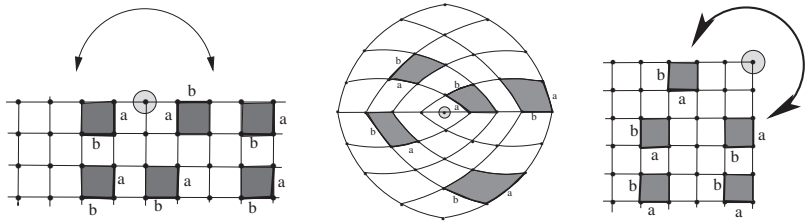

FIG. 9.7 – Construction of the rotational disclination by removing the solid angle π (Left) and $3\pi/2$ (Right). The reconstructed lattice after removing the π solid angle (center).

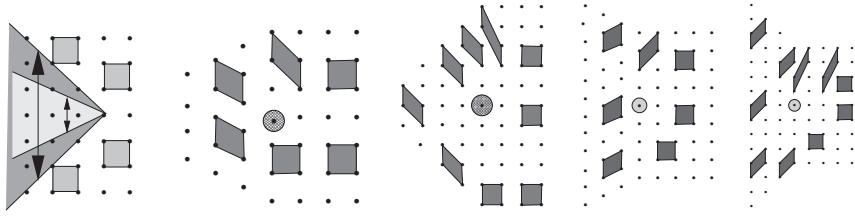

FIG. 9.8 – Construction of the angular dislocation by removing or adding one of the solid angles shown on the left picture. Reconstructed lattices after removing or adding small or large sectors are shown together with transport of the elementary cell along a closed path around the defect on the reconstructed lattice. The identification of boundaries after removing or adding a solid angle is done by the parallel shift of lattice points in the vertical direction.

systems as a defect of regular lattices associated with focus-focus singularities (see next subsection).

9.5 Lattices in phase space. Dynamical models. Defects.

Lattices appear naturally not only in the configuration space, as localized positions of atoms or more complicated particles. We turn now to dynamical systems, in particular to Hamiltonian systems. The basic object of our study is the phase space formed by conjugated position and momentum variables. The notion of integrable classical system leads to the appearance of toric fibrations.

The most evident appearance of lattices is associated with quantization of classical Hamiltonian integrable systems. Integer values of actions correspond to quantum states forming local lattices of quantum states.

Integrable problem in classical mechanics and corresponding quantum problems are very special to be associated directly with concrete physical systems. Certain qualitative features of integrable classical problems inherited also by quantum systems remain valid after small deformation because of their topological origin. This justifies the study of integrable systems from the point of view of further analysis of generic (non-integrable) systems.

To see the relation of regular lattices and their defects to dynamical systems we can start with one-degree of freedom problem. The Hamiltonian system describing the motion of a particle in a one dimensional potential can be imagined for simplicity as harmonic or slightly anharmonic oscillator.

Near the minimum of the potential the classical phase portrait shown in Figure 9.9, e can be topologically described as a system of circles (Figure 9.9, a), fibered over an interval and a singular fiber, a point, associated with the boundary point, the minimum. The corresponding system of quantum levels is a sequence of points which can be deformed to a regular one-dimensional lattice (with a boundary) associated to the harmonic oscillator (9.9, b). Small deformations of the one-dimensional problem cannot change qualitatively neither classical fibration, nor the lattice of quantum states. Qualitative modification of classical fibration is related with bifurcation of the phase portrait associated with the appearance of new stationary points on the energy surface. Subfigure 9.9, f shows qualitatively new phase portrait after the bifurcation associated with the formation of two new stationary points and the separatrix. Classical fibration 9.9, c now has a singular fiber (associated with a separatrix) and three regular regions, associated with locally defined lattices.

Completely integrable classical Hamiltonian for a two-degree of freedom system can be represented by its two-dimensional energy momentum (EM) map each regular point of which is associated with a regular T^2 fiber. The corresponding quantum system is characterized by the joint spectrum of two mutually commuting integrals of motion. In the case of the two-dimensional isotropic harmonic oscillator (see Figure 9.10) two integrals of motion can be chosen as the energy E, which is the eigenvalue of the Hamiltonian H and the projection of angular momentum m which is the eigenvalue of L_z.

$$H = \frac{1}{2}(p_1^2 + q_1^2) + \frac{1}{2}(p_2^2 + q_2^2), \tag{9.1}$$

$$L_z = p_1 q_2 - p_2 q_1. \tag{9.2}$$

Their joint eigenvalues form a regular two-dimensional lattice bounded by two rays.

Along with special fibers associated to boundary lines of the energy-momentum map, it is possible that integrable fibrations have also singular fibers inside the energy momentum map. Typical images of energy momentum

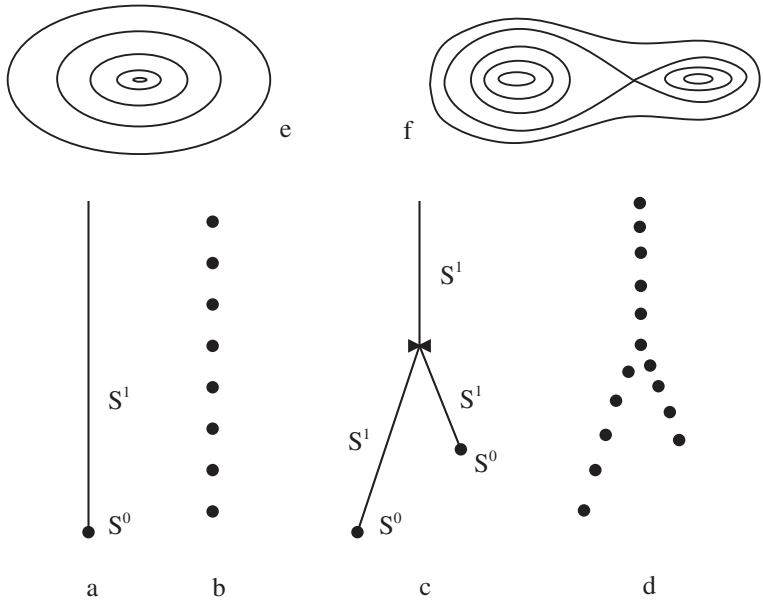

FIG. 9.9 – Classical and quantum bifurcations for the one degree of freedom system. Situations before (a,b,e) and after (c,d,f) the bifurcation are shown. (a) Energy map for a harmonic oscillator type system. Inverse images of each point are indicated. (b) Quantum state lattice for a harmonic oscillator type system. (c) Energy map after the bifurcation. Inverse images of each point are indicated. (d) Quantum state lattice after bifurcation represented as composed of three regular parts glued together. (e) Phase portrait for a harmonic oscillator type system. Inverse images are S^1 (generic inverse image) and S^0 - inverse image for a minimal energy value. (f) Phase portrait after bifurcation.

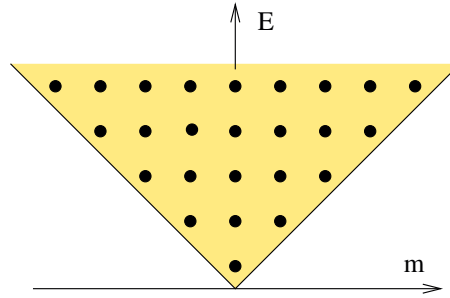

FIG. 9.10 – Joint spectrum of two commuting operators (9.1, 9.2) together with the image of a classical EM map for a two-dimensional isotropic harmonic oscillator.

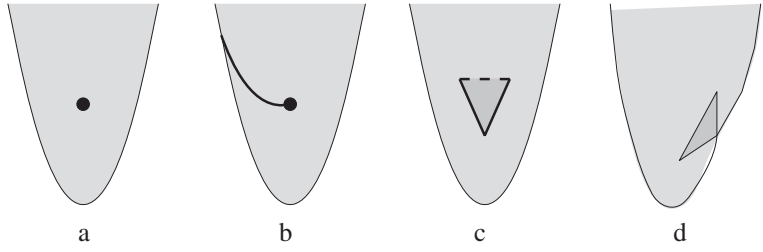

FIG. 9.11 – Typical images of the energy momentum map for completely integrable Hamiltonian systems with two degrees of freedom in the case of: (a) integer monodromy, (b) fractional monodromy, (c) nonlocal monodromy, and (d) bidromy. Values in the lightly shaded area lift to single 2-tori; values in darkly shaded area lift to two 2-tori.

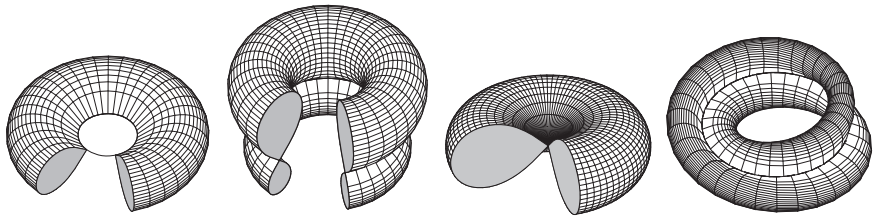

FIG. 9.12 – Two dimensional singular fibers in the case of integrable Hamiltonian systems with two degrees of freedom (left to right): singular torus, bitorus, pinched and curled tori. Singular torus corresponds to critical values in Figure 9.11 (c,d), (ends of the bitorus line). Bitorus corresponds to critical values in 9.11 (c,d), which belong to the singular line (fusion of two components). Pinched torus correspond to the isolated focus focus singularity in Figure 9.11 (a). Curled torus is associated with the critical values at the singular line in Figure 9.11 (b), (fractional monodromy).

maps possessing singular fibers for the two-degree-of-freedom Hamiltonian systems are shown in Figure 9.11. Visualization of singular fibers is given in Figure 9.12. The presence of singular fibers can be considered for classical fibration as a singularity which naturally influences the regular character of the fibration. For corresponding quantum systems regular regions of classical fibration correspond to locally regular lattices of common eigenvalues of mutually commuting operators. Singular fibers result in formation of defects of lattices of common eigenvalues.

For integrable systems with two-degrees of freedom the simplest codimension two singularity of the energy momentum map is the so called focus-focus point associated with a pinched torus. Its manifestation on the joint spectrum lattice for the corresponding quantum problem is shown in Figure 9.13 on the

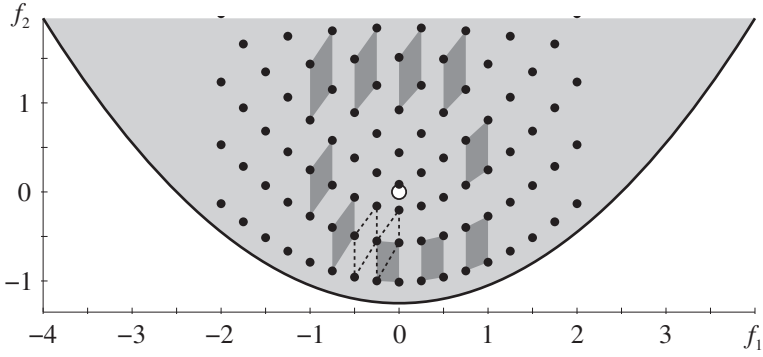

FIG. 9.13 – Joint spectrum of two commuting operators together with the image of the classical EM map for the resonant $1:(-1)$ oscillator [80]. Quantum monodromy is seen as a result of transportation of the elementary cell of the quantum lattice along a closed path through a non simply connected region of the regular part of the image of the EM map.

example of the resonant $1:(-1)$ oscillator. The two mutually commuting integrals of motion for this example are given by

$$f_1 = \frac{1}{2}(p_1^2+q_1^2)-\frac{1}{2}(p_2^2+q_2^2), \tag{9.3}$$

$$f_2 = p_1q_2+p_2q_1+\frac{1}{4}(p_1^2+q_1^2+p_2^2+q_2^2)^2. \tag{9.4}$$

It is clear that outside a small neighborhood of a codimension-2 defect the lattice of common eigenvalues remains regular, i.e. it can be transformed (within a local simply connected region of the image of the energy momentum map) to a simple square lattice by an appropriate choice of variables (local actions). At the same time the existence of a singularity imposes that along a closed path surrounding the singularity the unique choice of action variables does not exist. The evolution of the elementary cell of the local lattice along a path surrounding the singularity leads to a new choice of local action variables. Transformation between initial and final choices of local action variables is named a quantum monodromy. The type of quantum monodromy depends on the type of singularity of integrable classical fibration. The simplest singularity of classical integrable fibration, i.e. singly pinched torus, corresponds to transformation of the basis of the elementary cell of the quantum lattice by the matrix M

$$M=\begin{pmatrix}1 & 0\\ 1 & 1\end{pmatrix}, \tag{9.5}$$

which is defined up to the $SL(2,Z)$ transformation.

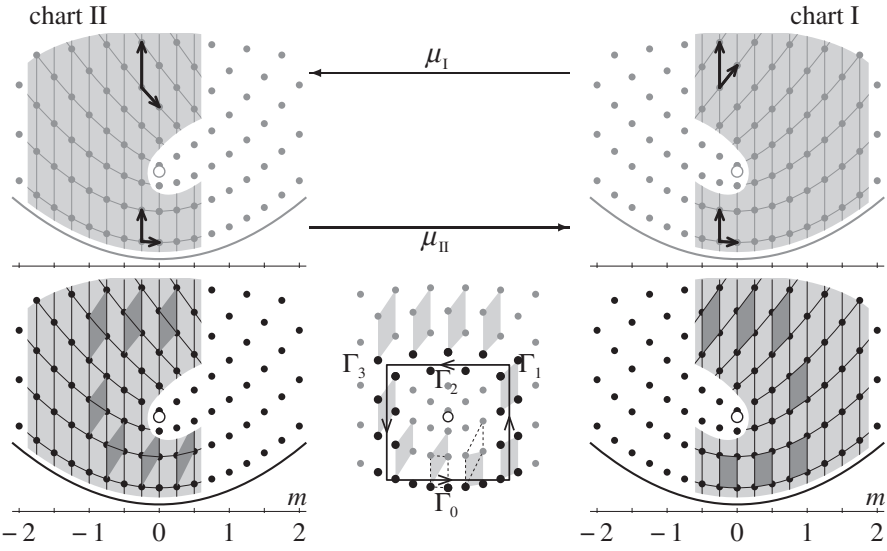

FIG. 9.14 – Two chart atlas which cover the quantum lattice of the $1 : (-1)$ resonant oscillator system represented in Figure 9.13. Top plots show the choice of basis cells and the gluing map between the charts. Bottom plots show the transport of the elementary cell (dark grey quadrangles) in each chart. Central bottom panel shows the closed path Γ and its quantum realization (black dots) leading to nontrivial monodromy (compare with Figure 9.13).

A possible choice of two overlapping simply connected charts with associated evolution of elementary cells for each chart is used in Figure 9.14 to explain the appearance of quantum monodromy for a lattice with a defect. Among the different possible visualizations of such simple-monodromy defect the most natural is that represented in Figure 9.15. Its construction is similar to that used for the "angular dislocation defect" shown in Figure 9.8. The idea of the construction of the defect is as follows. We cut from the regular lattice a wedge shown in Figure 9.14, left, and identify points on the two boundary rays of the cut. The wedge is chosen in such a way that the number of removed points from the lattice is a linear function of the integral of motion. After identification of the boundaries of the cut the reconstructed lattice remains regular except in the neighborhood of a singular point and is characterized by a quantum monodromy matrix (9.5).

Along with codimension-2 singularities classical fibrations for integrable dynamical systems have codimension-1 singularity lines. Such singularity is associated, for example, with a curled torus (see Figure 9.12) and can be studied on a concrete example of the two-dimensional nonlinear $1 : (-2)$ resonant oscillator.

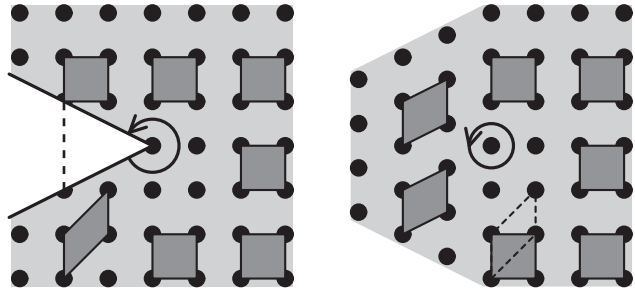

FIG. 9.15 – Construction of the 1:(−1) lattice defect starting from the regular Z^2 lattice. The solid angle is removed from the regular Z^2 lattice and points on the so obtained boundary are identified by vertical shifting. Dark grey quadrangles show the evolution of an elementary lattice cell along a closed path around the defect point.

Two integrals of motion for this problem are given by

$$f_1 = \frac{\omega}{2}(p_1^2 + q_1^2) - \frac{2\omega}{2}(p_2^2 + q_2^2) + R_1(q,p), \tag{9.6}$$

$$f_2 = Im[(q_1 + ip_1)^2(q_2 + ip_2)] + R_2(q,p). \tag{9.7}$$

Here R_i are higher order terms which ensure the compactness of the subspaces with fixed energy. The corresponding image of the energy momentum map together with the lattice of the joint quantum spectrum are shown in Figure 9.16.

The new qualitative feature which appears with this example is the possibility to define a generalization of quantum monodromy in case when the closed path on the image of the energy-momentum map crosses the line of singularities. The construction of the defect by the cutting and gluing procedure of a regular lattice is shown in Figure 9.17. The key point now is the possibility to go to sublattice (of index two in this concrete case) and to show that it is possible to define what happens with the elementary cell when crossing the line of singularities. At the same time being in regular region, it is possible to return to the original elementary cell. The monodromy matrix written in this case for an elementary initial cell includes fractional entries. That is why the corresponding qualitative feature was named fractional monodromy.

9.6 Modular group

In order to see the relation between lattices and functions of complex variables let us remember that an elliptic function is a function f meromorphic

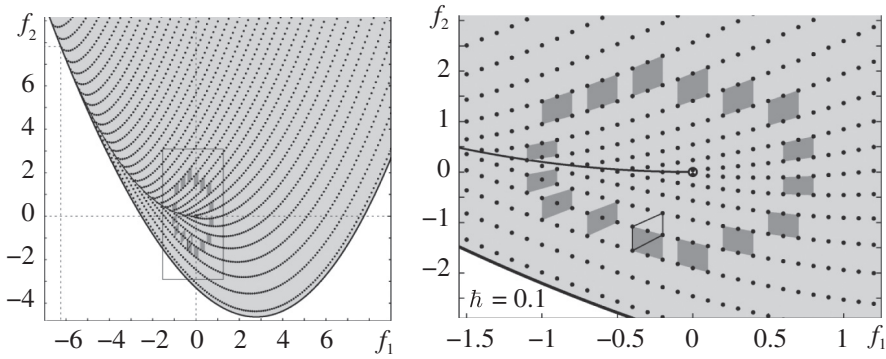

FIG. 9.16 – Joint quantum spectrum for two-dimensional nonlinear $1 : (-2)$ resonant oscillator [80]. The singular line is formed by critical values whose inverse images are curled tori shown in Figure 9.12. In order to get the unambiguous result of the propagation of the cell of the quantum lattice along a closed path crossing the singular line, the elementary cell is doubled.

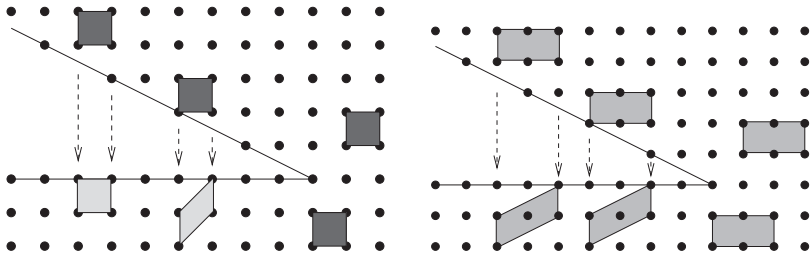

FIG. 9.17 – Representation of a lattice with a $1 : 2$ rational defect by cutting and gluing. Left: The elementary cell goes through cut in an ambiguous way. The result depends on the place where the cell crosses the cut. Right: Double cell crosses the cut in an unambiguous way.

on $\mathbb{C}$ for which there exist two non-zero complex numbers ω_1 and ω_2 with $\omega_1/\omega_2 \notin \mathbb{R}$, such that $f(z) = f(z + \omega_1)$ and $f(z) = f(z + \omega_2)$ for all z. Denoting the "lattice of periods" by $\Lambda = \{m\omega_1 + n\omega_2 \mid m, n \in \mathbb{Z}\}$, it follows that $f(z) = f(z+\omega)$ for all $\omega \in \Lambda$. The complex numbers (ω_1, ω_2) generating the period lattice are defined up to $SL(2, Z)$ transformation, like quadratic forms or bases of two-dimensional lattices. Note, that for two-dimensional real lattices the group describing the transformation of bases is often extended by including reflections. In such case the group is $GL_2(\mathbb{Z})$, which includes integer 2 by 2 matrices with determinant ± 1. In complex analysis the holomorphic transformations includes only those with positive determinant, whereas transformations with negative determinant are anti-holomorphic. This means that

under holomorphic transformations a pair of complex numbers (vectors) α_1, α_2 will generate exactly the same lattice as the lattice generated by ω_1, ω_2 if and only if

$$\begin{pmatrix} \alpha_1 \\ \alpha_2 \end{pmatrix} = \begin{pmatrix} a & b \\ c & d \end{pmatrix} \begin{pmatrix} \omega_1 \\ \omega_2 \end{pmatrix} \tag{9.8}$$

for some matrix in $SL_2(\mathbb{Z})$.

To compare with more general $GL(2, R)$ group, let us consider the action of the $GL(2, R)$ group on the complex plane $z \in \mathbb{C}$

$$z \in \mathbb{C}, \quad g = \begin{pmatrix} a & b \\ c & d \end{pmatrix} \in GL(2, R); \quad g \cdot z = \frac{az + b}{cz + d} \in \mathbb{C}. \tag{9.9}$$

We verify easily that

$$-I_2 \cdot z = z, \quad \Im(g \cdot z) = \frac{\det g}{|cz + d|^2} \Im(z). \tag{9.10}$$

These transformations show that the upper half part, $\mathcal{H}$, of the complex plane is invariant under transformations by $SL_2(\mathbb{R})$ matrices with a positive determinant. If we apply transformation with a negative determinant, the imaginary part of the complex number changes the sign.

In order to study the rational transformations of the upper half complex plane $\mathcal{H}$, which leave the period lattice invariant we need to be restricted to the $SL_2(\mathbb{Z})$ group rather than for a larger $GL_2(\mathbb{Z})$ one. Moreover, the element $-I_2 = \begin{pmatrix} -1 & 0 \\ 0 & -1 \end{pmatrix}$ from $SL_2(\mathbb{Z})$ acts trivially on $\mathcal{H}$. Thus, we can conclude that in fact it is the group $PSL_2(\mathbb{Z}) = SL_2(\mathbb{Z})/(\{\pm 1\}$ that acts. The subgroup $\{\pm 1\}$ is the center of the image of $SL_2(\mathbb{Z})$ in $PSL_2(\mathbb{Z})$.

The name modular group is reserved for the group

$$G = SL_2(\mathbb{Z})/\{\pm 1\},$$

which is the image of the group $SL_2(\mathbb{Z})$ in $PSL_2(\mathbb{R})$. But sometimes the discrete subgroup $SL_2(\mathbb{Z})$ of the group $SL_2(\mathbb{R})$ is also named a modular group.

The interest in the study of the lattices and modular group action on the upper half of the complex plane is related to the use of it as a model of hyperbolic space.

It is quite instructive to describe the fundamental domain of the modular group action on the upper half part of the complex plane and to compare the action of the modular group on the complex plane with the action of the $SL_2(\mathbb{Z})$ group on the cone of quadratic forms studied in chapter 6 in relation to the two-dimensional lattice classifications.

The choice of the fundamental domain of the modular group action is shown in Figure 9.18, where several images of the chosen fundamental domain under the modular group action are also shown. Special care should be taken for the indicated boundary of the fundamental domain in order to ensure that

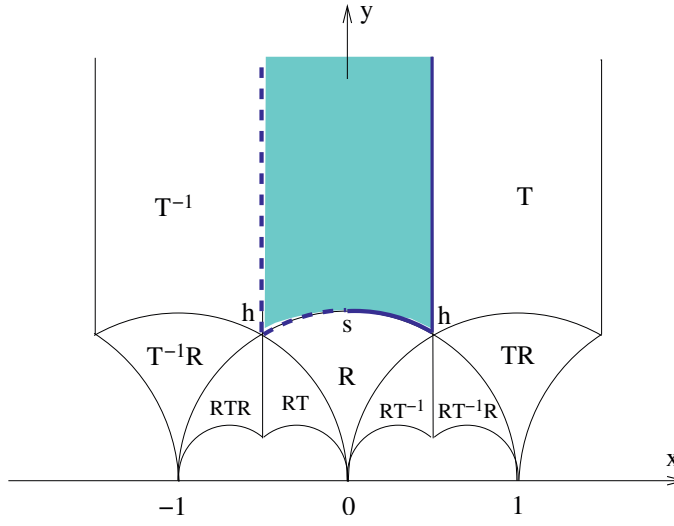

FIG. 9.18 – The fundamental domain of the modular group action on the upper half complex plane.

only one point from each orbit of the modular group action on the upper half of the complex plane is included in the fundamental region.

To describe the fundamental domain F let us represent it as a union of two subdomains $F = F^{(1)} \cup F^{(2)}$, where

$$F^{(1)} := \{z \in \overline{\mathbb{C}} : 0 \le \Re z \le \frac{1}{2}, \quad |z| \ge 1\}, \tag{9.11}$$

$$F^{(2)} := \{z \in \mathbb{C} : -\frac{1}{2} < \Re z < 0, \quad |z| > 1\}. \tag{9.12}$$

Here $\overline{\mathbb{C}}$ is the extended complex plane, note that ∞ is included in $F^{(1)}$ but not in $F^{(2)}$. The fundamental domain shown on Figure 9.18 by shading has boundaries marked by solid lines and boundaries marked by dashed lines. Only solid lines are included in the definition of the fundamental domain. To see the topology of the fundamental domain we need to identify two vertical boundaries and two halves of the circular boundary. The result is the topological sphere.

To see in more details the action of the modular group on the upper half complex plane let us introduce two generator of the $SL_2(\mathbb{Z})$ group.

Let

$$U = \begin{pmatrix} 1 & 1 \\ 0 & 1 \end{pmatrix}; \quad V = \begin{pmatrix} 0 & -1 \\ 1 & 0 \end{pmatrix}; \tag{9.13}$$

The corresponding mapping associated with the introduced action of $SL_2(\mathbb{Z})$ on the complex plane are given by

$$Uz = z + 1, \quad Vz = -1/z. \tag{9.14}$$

Let us note further that

$$U^k = \begin{pmatrix} 1 & k \\ 0 & 1 \end{pmatrix}; \quad V^2 = -I; \quad (VU)^3 = -I. \tag{9.15}$$

This means that from the point of view of the $SL_2(\mathbb{Z})$ group, V is a generator of a subgroup of order four, VU is a generator of a subgroup of order six.

But returning to the group of mappings on the upper half complex plane, i.e. to the $PSL_2(\mathbb{Z})$ group and taking into account the mentioned earlier fact that $-I$ acts trivially on the upper half complex plane (i.e. belongs to the center), we can say that the mapping V has order two and the mapping U has order three.

To characterize the fundamental domain we need to describe the stabilizers of different points belonging to the fundamental domain, i.e. find different strata of the group action. It can be checked [85] that all points have the trivial stabilizer except for point i denoted s on Figure 9.18, points $z = e^{\pi i/3}$, and $z = s^{2\pi i/3}$ denoted respectively as h and h' on Figure 9.18 and the ∞ point of the extended complex plane. Point i has a stabilizer generated by the element V, i.e. the stabilizer of point i is a group of order two. Two points $z = e^{\pi i/3}$, and $z = s^{2\pi i/3}$ belong to the same orbit. Their stabilizers are conjugate and generated by VU or by UV. The order of stabilizer is three. The ∞ point is invariant under the so called parabolic subgroup generated by element U. The corresponding discrete subgroup has infinite order. So finally we can say that the space of the orbits of the modular group action on the extended upper half complex plane $\mathcal{H}^*$ is a topological sphere with one point belonging to the stratum with the stabilizer being the group of order two and one point belonging to the stabilizer of order three and one point with stabilizer of infinite order.

9.7 Lattices and Morse theory

Many important physical characteristics of periodic crystals depend on the number and positions of stationary points of continuous functions defined on the Brillouin zone (see section 8.4). For three-dimensional crystals the Brillouin zone is a three-dimensional torus stratified by the action of the point symmetry group of the crystal. Morse theory is an appropriate mathematical tool which allows us to relate the number of stationary points of a smooth function with the topology of the space on which this function is defined. In the presence of symmetry additional restrictions on the number and position of stationary points follow from group action, in particular,

from the existence of zero-dimensional strata formed by critical orbits which are stationary points for any invariant smooth function. In this section we illustrate the application of Morse theory to the description of the minimal possible system of stationary points for functions invariant with respect to point groups of 14 three-dimensional Bravais classes.

9.7.1 Morse theory

We start with short reminder of Morse theory. Let us consider a smooth real valued function f on a real compact manifold M of dimension d. If in a local coordinate system $\{x_i\}$, $1 \le i \le d = \dim M$, defined in a neighborhood of a point $m \in M$ the function f satisfies equations

$$\frac{\partial f}{\partial x_i} = 0; \quad \det \frac{\partial^2 f}{\partial x_i \partial x_j} \neq 0, \tag{9.16}$$

of vanishing gradient and non-vanishing determinant of the Hessian, we say that f has a non degenerate extremum at m. By a change of coordinates $\{x_i\} \mapsto \{y_i\}$ in a neighborhood of m the function can be transformed into $f = \sum_i \varepsilon_i y_i^2$ with $\varepsilon_i = \pm 1$. The number of "minus" signs is independent of the coordinate transformation. It is called the Morse index μ of this non degenerate extremum: for instance $\mu = 0$ for a minimum, $\mu = d$ for a maximum, and the intermediate values correspond to the different types of saddle points. By a small generic deformation all stationary points can be made non degenerate. A function on M with all its extrema non degenerate is called a Morse function. The essence of Morse theory is the relations between the numbers c_k of extrema of Morse index k and the topological invariants of the manifold M, its Betti numbers. The Betti number b_k is defined as the rank of the k-th homology group of M. Intuitively b_k is the maximal number of k-dimensional submanifolds of M which cannot be transformed into one another or into a submanifold of smaller dimension. For instance for the sphere S_d of dimension d, $b_0 = b_d = 1$ and all the other b_k vanish. More generally one has the Poincaré duality: $b_k = b_{d-k}$. The information about Betti numbers can be written in a form of a Poincaré polynomial $P_M(t)$ of a manifold M

$$P_M(t) = \sum_{i=0}^{d} b_k t^k; \quad d = \dim(M); \quad \text{e.g. } P_{S_d}(t) = 1 + t^d. \tag{9.17}$$

The Poincaré polynomial of a topological product of manifolds is the product of the Poincaré polynomials of the factors. For instance, a d-dimensional torus is the topological product of d circles. This gives the Betti numbers for the d-dimensional torus T_d:

$$T_d = S_1^d \Rightarrow P_{T_d}(t) = (1+t)^d \Rightarrow b_k(T_d) = \binom{d}{k}. \tag{9.18}$$

For a compact manifold M the system of Morse relations consists of one equality

$$\sum_{k=0}^{d}(-1)^{d-k}(c_k - b_k) = 0 \quad \Leftrightarrow \quad \sum_{k=0}^{d}(-1)^{d-k}c_k = \sum_{k=0}(-1)^{d-k}b_k \stackrel{\text{def}}{=} \chi(M), \tag{9.19}$$

where $\chi(M)$ is the Euler Poincaré characteristic, and the system of inequalities

$$\sum_{k=0}^{\ell}(-1)^{\ell-k}(c_k - b_k) \geq 0, \quad 0 \leq \ell < d, \tag{9.20}$$

which can be simplified to a more crude form $c_k \geq b_k$. These simplified inequalities are not equivalent to Morse inequalities (9.20) but give lower bounds to the number of extrema of a Morse function.

For functions defined on the Brillouin zone (i.e. for a torus) for $d = 2$ and $d = 3$ the relations (9.19), (9.20) become

$$\begin{aligned} d = 2, \quad & c_0 - c_1 + c_2 = 0, \quad c_0 \geq 1 \leq c_2, \quad c_0 + 1 \leq c_1 \geq c_2 + 1, \\ d = 3, \quad & c_0 - c_1 + c_2 - c_3 = 0, \quad c_0 \geq 1 \leq c_3, \quad c_1 \geq c_0 + 2, \quad c_2 \geq c_3 + 2. \end{aligned} \tag{9.21}$$

Thus for the two-dimensional torus the minimal number of stationary points for a Morse function cannot be smaller than four, whereas for the three-dimensional torus the minimal number is eight.

9.7.2 Symmetry restrictions on the number of extrema

In the presence of symmetry acting on a manifold all stationary points belonging to the same orbit of the group action naturally have the same Morse index. Moreover for invariant functions all orbits isolated in their strata should be formed by stationary points. Such orbits are named *critical orbits*. These stationary points are fixed (their position does not vary under small deformation of the Morse function). Thus in the presence of symmetry it is quite useful to find first all critical orbits and then verify if some other stationary points should exist in order to satisfy Morse inequalities.

Before passing to the application of the Morse analysis for functions defined on the Brillouin zone for different point symmetry groups we consider two simpler examples for a function defined on the two-dimensional sphere in the presence of symmetry. In the case of the O_h group action on the sphere (see section 4.5.1, Figure 4.20) there are three critical orbits: one consists of 6 points (stabilizer C_{4v}), another of 8 points (stabilizer C_{3v}), and the third one is formed by 12 points (stabilizer C_{2v}). We have 26 fixed stationary points among which points with C_{4v} and C_{3v} stabilizers should be stable, i.e. to be maxima or minima and cannot be saddles. One can easily verify that six maxima/minima, eight minima/maxima and 12 saddles satisfy

Morse inequalities and consequently the minimal number of stationary points for a Morse function on the sphere in the presence of O_h symmetry is 26.

As another example let us study the Morse function of the sphere in case of the C_{2h} point group action. There is only one critical orbit of the C_{2h} group action consisting of two points (see section 4.5.1, Figure 4.17). These two points should have the same Morse index. In order to construct a Morse function with the minimal number of stationary points it is necessary to add two orbits of two points located on C_h stratum. Positions of stationary points on one-dimensional stratum are not fixed and the distribution of stationary points among these three orbits is arbitrary. The only condition imposed by the Morse relation for the function invariant under C_{2h} action and possessing the minimal possible number of stationary points is the existence of two equivalent minima, two equivalent maxima and two equivalent saddles.

As a crystallographic application we give here the list of critical orbits and the minimal number of stationary points for functions defined on the Brillouin zone (three-dimensional torus) in the presence of point symmetry group action for 14 Bravais classes. The results of the analysis are represented in the form of Table 9.2 taken from [72]. For each of the 14 Bravais classes given in the first column we list in columns 2-6 all critical orbits classified by their k-values. Eight points corresponding to $k = 0$ (one point) and to $2k = 0$ (seven points) are critical for all Bravais classes. Under the presence of symmetry seven points associated with the $2k = 0$ form orbits consisting of one or several equivalent points. The numbers of critical points in each individual orbit of the symmetry group action are shown in column 3. For points with higher local symmetry (i.e. for $nk = 0$ with $n = 3, 4, 6$) columns labeled by $nk = 0$ indicate the number of critical points within the corresponding orbit of the group action. The points between [] have to be maxima or minima. The column labeled "nb" gives the minimal possible number of stationary points for each Bravais class. This number for two Bravais classes, namely for $Fmmm$ and $Im\bar{3}m$, is larger than the number of stationary points associated with critical orbits. These additional stationary points which are obliged to exist for the Morse functions are indicated explicitly as $n_{\mathrm{crit}} + n_{\mathrm{non-crit}}$.

Finally, the last four columns give the possible distribution of stationary points into subsets of stationary points with a given Morse index. Several lines give alternative distributions for the simplest Morse type functions, i.e. for Morse type functions with the minimal number of extrema.

TAB. 9.2 – List of the critical orbits on the Brillouin zone for the action of point symmetry group G of the 14 Bravais classes and the numbers and Morse indices of extrema of G-invariant functions with the minimum number of stationary points. Columns "nk" give the number of critical points satisfying the $nk = 0$ condition. See text for further details.

Bravais class	0	$2k$	$4k$	$3k$	$6k$	nb	0, 3	1, 2	2, 1	3,0
$P\bar{1}$	1	1,1,1,1,1,1,1				8	1	1+1+1	1+1+1	1
$P2/m$	1	1,1,1,1,1,1,1				8	1	1+1+1	1+1+1	1
$C2/m$	1	1,1,1,2,2				8	1	1+2	1+2	1
$Pmmm$	1	1,1,1,1,1,1,1				8	1	1+1+1	1+1+1	1
$Cmmm$	1	1,1,1,2,2				8	1	1+2	1+2	1
$Fmmm$	1	1,1,1,4				8+2	1	4	1+1+2	1
							1+1	4	1+2	1
$Immm$	1	1,2,2,2	2			10	1	2+2	2+2	1
							2	2+2	1+2	1
$P4/mmm$	1	1,1,1,2,2				8	1	1+2	1+2	1
$I4/mmm$	1	1,2,4	2			10	1	4	2+2	1
							2	4	1+2	1
$R\bar{3}m$	1	1,3,3				8	1	3	3	1
$P6/mmm$	1	1,3,3		2	2	12	1	2+3	2+3	1
							2	2+3	1+3	1
							2	1+3	1+3	2
							3	2+3	1+2	1
$Pm\bar{3}m$	[1]	1,3,3				8	1	3	3	1
$Fm\bar{3}m$	[1]	3,4	6			14	1	3	6	4
							1	4	6	3
$Im\bar{3}m$	[1]	1,6	[2]			10+6	1	6	1+6	2
							2	6	6	1+1